Suhasini et al.

A phosphodiesterase 4B-dependent interplay between tumor cells and the microenvironment regulates angiogenesis in B-cell lymphoma

Supplementary Materials and Methods:

Cell lines, primary DLBCL and compounds. Human DLBCL cell lines (SU-DHL4, SU-DHL6, SU-DHL10, OCI-Ly4, OCI-Ly10 and OCI-Ly18) were cultured at 37^0C, 5% CO2 in RPMI-1640 medium supplemented with 10%-20% fetal bovine serum (FBS), 100U/ml penicillin, 100ug/ml streptomycin, 2mM L-gutamine and 10 mM N-2-hydroxyethylpiperazine-N'-2-ethanesufonic acid (HEPES) buffer. Paired paraffin blocks and RNA were available from 28 untreated DLBCL patients, obtained de-identified from our local tumor bank. The use of these anonymized samples was approved by the Institutional Review Board of University of Texas Health Science Center San Antonio. Forskolin and Roflumilast were purchased from LC laboratories (Woburn, MA) and Santa Cruz Biotechnology (Dallas, TX), respectively, and 8-Bromoadenosine 3',5'-cyclic monophosphate (8-Br-cAMP) was obtained from Sigma (St. Louis, MO).

Mice. The *Pde4b* knockout mouse (B6N;129P2-*Pde4b*^{tm1Mct}/Mmucd), herein referred to as *Pde4b-/-*, has been described before[1] and was obtained from the Mutant Mouse Regional Repository Center (MMRRC, University of California, Davis); the knockout alleles in this strain were previously transferred to a C57BL/6 background by backcrossing over 13 generations. A local colony was maintained by crossing *Pde4b+/-* mice. The B6.Cg-Tg(IghMyc)22Bri/J hemizygous mice, herein referred to as *Eμ-Myc-Tg*, was obtained from the Jackson Laboratory (Bar Harbor, ME). A local colony was maintained by breeding hemizygous *Eμ-Myc-Tg* males with wild-type C57BL/6 females. To generate the composite *Pde4b-/-; Eμ-Myc-Tg* mice, we first bred *Pde4b+/-* females to *Eμ-Myc-Tg* males; subsequently, *Pde4b+/-* females were crossed to *Pde4b+/-;MycTg* males, creating the desired *Pde4b-/-;Eμ-Myc-Tg* transgenic strain; *Pde4b +/+;Eμ-Myc-Tg* mice served as controls in the relevant experiments. All mice were monitored three times a week for lymphoma development, often defined by enlarged cervical and brachial lymph nodes resulting in the characteristic 'water wings' appearance[2]. Mice were sacrificed

when tumors became larger than 1 cm, or if signs of systemic disease were present (hunched posture, slow movement, ruffled fur, or hind-limb paralysis). Lymphomas were harvested and immediately processed for histopathological and immunophenotypic studies. Tumors were also flash frozen as viable single-cell suspensions or intact tissue. The immunophenotype of viable cells (7AAD-negative) lymphoma cells was defined by fluorescence-activated cell sorter (FACS) analysis, using APC-conjugated anti-mouse B220 (eBiosciences), FITC-conjugated anti-mouse immunoglobulin M (IgM) (BD Pharmingen), and isotype controls. The LSR II (BD Biosciences) instrument was used for acquisition and data analyses performed the FACSDiva Software (BD Biosciences). All mice were maintained in specific pathogen-free conditions, and experimental procedures were approved by the Institutional Animal Care and Use Committee of the University of Texas Health Science Center San Antonio.

Genetic modulation of PDE4B and AKT in DLBCL cell lines. The generation of SU-DHL6 cells expressing PDE4B-WT, PDE4B-phophodiesterase inactive (PI) mutant (both FLAG-tagged), constitutively active, myristoylated, AKT (CA-AKT) or empty vector (murine stem cell virus-enhanced green fluorescent protein [MSCV-eGFP]) was reported earlier[3]. For loss of function assays, PDE4B was transiently knocked-down in the PDE4B-high DLBCL cell line OCI-Ly18 using a small interfering RNAs (siRNAs) strategy, as described earlier[4]. Confirmation of the *PDE4B* knockdown was performed with quantitative real-time reverse transcription polymerase chain reaction (Q-RT-PCR) and western blotting, which were also used for quantification of PDE4B expression in the DLBCL parental cell lines, as we described[5]. Lastly, *PDE4B* expression in primary DLBCL biopsies was determined by Q-RT-PCR.

Western blotting. Whole-cell lysates were extracted from DLBCL cell lines or primary murine tumors, separated by sodium dodecyl sulfate-polyacrylamide gel electrophoresis (SDS-PAGE), and transferred to polyvinylidene difluoride membrane, as described [6]. Thereafter, they were examined with antibodies directed to PDE4B (H-56, Santa Cruz Biotechnology), total AKT and phospho-AKT (Thr 308) (all from Cell Signaling, Beverly, MA), FLAG or β-actin (both from Sigma Aldrich, St Louis, MO).

Quantification of vascular endothelial growth factor A (VEGFA). VEGFA abundance was examined at RNA and protein levels, in human and murine samples. For quantification of the *VEGFA* gene expression, RNA was isolated from DLBCL cell lines following 6h exposure to Forskolin or vehicle control, cDNA generated, and real-time RT-PCR performed as described previously[7] . The *VEGFA* expression was normalized to that of the housekeeping control gene *TBP* (TATA-binding protein). The relative quantification was achieved by calculating ΔΔCT, and expression was defined as $2^{-\Delta\Delta CT}$, as we reported [8]. The primer sequences are listed in Supplementary Table 2. Quantification of secreted VEGFA was performed using Human or Mouse VEGF Immunoassay according to the manufacturer's recommendations (R&D systems, Minneapolis, MN). In brief, genetically modified or parental DLBCL cell lines were exposed to Forskolin or vehicle control in presence or absence of Roflumilast for 6h, followed by drug wash-off, replenishment with fresh drug-free media, and supernatants collection after 24h. For the murine assays, VEGF was quantified in the sera collected immediately after lymphoma bearing mice (n=30) were sacrificed.

Quantification of intracellular cAMP. Intracellular cAMP levels were measured as we previously described[4]. In brief, after exposure to the adenylyl cyclase activator Forskolin (40 μM, for 30 minutes) or DMSO, DLBCL cell lines were harvested and washed with PBS. cAMP was measured using enzyme-linked immunosorbent assay (ELISA) according to the manufacturer's instructions (Parameter cAMP assay; R&D Systems, Minneapolis, MN). cAMP was also measured in all conditioned media utilized in the HUVEC tube formation assay.

HUVEC tube formation assay. The HUVEC tube formation assays were performed on low passage sub-confluent human umbilical vein endothelial cells (HUVEC, Life Technologies). In brief, 3 x 10^4 HUVECs mixed with DLBCL cell line conditioned media were seeded in 48-well plates coated with basement membrane matrix (Geltrex, Life Technologies). After 4 to 5 hours incubation, the tube-like structure formations were captured using an inverted microscope (200× magnification) (Olympus). The total tube length, branch points and loops from three independent fields were quantified using Image J software[9]. Importantly, we established

several safeguards to guarantee the robustness of the HUVEC data. First, after exposure to Forskolin, the culturing media of the DLBCL cell lines was removed, the cells extensively washed, and replenished with Forskolin/Roflumilast-free fresh media, which was collected 24h later to be used in the HUVEC assays. In addition, we quantified the levels of cAMP in these conditioned media and found it to be nearly undetectable (sub-pmol amounts) across all cell lines examined, irrespective of whether the cells had been exposed to Forskolin and/or Roflumilast (Supplementary Figure 3). Thus, these conditioned media are drug- and cAMP-free, indicating that the HUVEC assays are reflective of the effects of Forskolin/cAMP/Roflumilast on the production of VEGF by the lymphoma cells, and not from a fortuitous presence of these Forskolin, Roflulimast or cAMP in the conditioned media.

Adoptive Transfer assays. Four cohorts of 6-8 week old female C57BL/6 mice (n= 60) were transplanted with lymphoma cells (1 x 10^6 cells injected in the tail vein) derived from unique B cell lymphomas that developed in four distinct *Pde4b+/+; Eμ-Myc-Tg* mice. In three cohorts (n=24), mice were monitored daily and upon clinical evidence of lymphoma (detected on average 10 days after transplant) randomized to receive the FDA-approved PDE4 inhibitor Roflumilast (5mg/Kg/day, by gavage) or vehicle control. These mice were sacrificed after 5 days of treatment, and lymphomas collected for histopathological and additional studies. In the last cohort (n=36), on the 5^{th} day post-transplant, before clinical evidence of lymphoma, the mice were randomized to Roflumilast (5mg/Kg/day by gavage) or vehicle control groups. The end-point of this cohort was survival and mice were sacrificed when signs of severe systemic disease were present (enlarged nodes, hunched posture, slow movement, ruffled fur, hind-limb paralysis) or after 30 days of drug administration, whichever came first. All mice were examined post-mortem, sera collected, and cervical, brachial and inguinal lymph nodes harvested.

PI3K assay. Quantification of PI3K activity was performed on whole-cell lysates collected from DLBCL cell lines or primary murine lymphomas, utilizing an ELISA-based assay (Echelon Biosciences). In brief, whole-cell extracts (50μg) were added to a mixture of PI(4,5)P2 substrate and reaction buffer containing adenosine triphosphate (ATP) and allowed to incubate at room

temperature for 2-3 hours. The reaction was stopped by adding PI(3,4,5)P3 detector mixed with EDTA (ethylenediaminetetraacetic acid) and transferred to a PI3K ELISA plate. The wells were washed and incubated with secondary detector. Following additional washes and reaction termination the plates were read at 450 nm on a FLUOStar OPTIMA 96-well plate reader (BMG Labtech). To calculate the PI3K activity we used nonlinear regression to construct a PI(3,4,5)P3 standard sigmoidal curve with variable slope. Thereafter, we interpolated the absorbance values from each sample thus defining the amount of PI(3,4,5)P3 generated (i.e., PI3K activity) in each sample. The assays performed in parental DLBCL cell lines included activation of the B-cell receptor (BCR) for 10 minutes with 10µg/ml of goat anti-human IgM/IgG (Jackson Immunoresearch, West Grove, PA).

Histopathology. Murine lymphomas: Enlarged cervical lymph nodes were fixed in formalin, processed, embedded in paraffin, and 4-µm serial sections obtained. One section was stained with hematoxylin and eosin (H&E) and the slides were reviewed by the pathologists to confirm the presence of malignant lymphoma. Immunohistochemistry (IHC) was performed on deparaffinized 4-µm sections for vWF (rabbit polyclonal anti-vWF, A0082, DAKO), CD34 (rabbit monoclonal anti-CD34, clone EP373Y, abcam) and VEGF (rabbit polyclonal anti-VEGF, ab46154, abcam). Manual staining for vWF (dilution 1:750) and CD34 (1:200) was performed after heat-induced epitope retrieval (HIER) in Reveal (Biocare Medical). Detection for vWF was completed using Mach 2 (Biocare Medical) with alkaline phosphatase and Warp Red (Biocare Medical) chromogen, and for CD34 using Mach 3 (Biocare Medical) with horseradish peroxidase (HRP) and Diaminobenzidine (DAB) chromogen. Automated staining for VEGF was performed after HIER in CC1 (Ventana Medical Systems), followed by detection using iView (Ventana Medical Systems) with HRP and DAB chromogen. All immunohistochemical sections were counterstained with hematoxylin.

Slides stained for vWF and CD34 were digitally scanned using an Aperio CS-O (Leica Biosystems) and examined in a blinded fashion by the pathologists (KNH and AWM) for microvessel density (MVD) quantification using AperioImageScope software (Leica Biosystems).

Immunohistochemically stained sections were examined at 100x magnification to identify areas of maximal MVD ("hot spots"). For each case, 3 hot spots were examined at 200x magnification (each field with an area of 1.14 mm2) and all microvessels manually counted and highlighted using the ImageScope software, which calculated the area of each vessel. Hot spots were counted within the lymph node tissue and areas of extranodal spread (defined as clearly outside the lymph node capsule and infiltrating adjacent fibro-adipose tissue) were excluded from the analysis. As previously defined [10], all endothelial cells or endothelial cell clusters, with or without a lumen, that were clearly separate from adjacent microvessels were counted as one microvessel. Vessels with muscular walls were not counted. The total microvessel count of each hot spot was calculated and data reported as the mean counts of the three hot spots per 200x field for each case. As indicated, to determine MVD, we initially stained the murine lymphomas with vWF and CD34. Comparison of these two approaches in multiple independent tumors indicated that a larger number and total area of vessels were stained for CD34 than for vWF antibody, a finding previously reported in non-Hodgkin lymphoma [11]. Further, although we found a good correlation between the vessel numbers defined by these two measurements (r=0.67, Pearson correlation coefficient), CD34 showed a more uniform staining, whereas vWF was overall fainter with more variable intensity. Thus, we selected CD34 staining as the marker of MVD in our series, as reported by others studying lymphomas and additional hematologic neoplasms[12-15]. Finally, VEGF immunostained slides were examined in a blinded fashion by pathologists and the staining intensity was scored in a semi-quantitative manner with a range from 0 to 4+. As for every VEGF positive tumor nearly all lymphoid cells were positive, this score reflects only intensity of VEGF expression, and not the percentage of positive cells in the biopsy.

Human DLBCL: Formalin-fixed paraffin-embedded blocks from 28 DLBCL patients were obtained from the institutional tumor bank. H&E slides from each case were reviewed by pathologist to confirm the diagnosis of DLBCL. Immunohistochemistry was performed on deparaffinized 4-µm sections for CD34 (mouse monoclonal anti-CD34, clone 8G12, BD Biosciences). Automated staining for CD34 (1:20 dilution) was performed after HIER in CC1 (Ventana Medical Systems), followed by detection using iView (Ventana Medical Systems) with HRP and DAB chromogen

and counterstaining with hematoxylin. Immunohistochemically stained slides for CD34 were digitally scanned and analyzed as described above. For the human DLBCLs, hot spots were chosen from areas with sheets of large neoplastic lymphocytes and as few intervening small lymphocytes as possible. Further, as delineated before in a large study of more than 200 primary DLBCLs[16], total microvascular area rather than the number of vessels per area is a more robust determinant of MVD in this tissue. Thus, in the human primary DLBCLs the MVD was defined as the sum of all microvessel areas divided by the total area analyzed (three hot spots = 3.42 mm2).

Statistics: Statistical analyses were performed with two-tailed Student's t test, one-way analysis of variance (ANOVA) with Bonferroni's post-test, linear regression analysis and the Spearman's rank correlation coefficient. Survival probably was estimated with a Kaplan-Meier analysis and the significance of the differences determined with the log-rank (Mantel–Cox) test. $P < 0.05$ was considered significant. Data analyses were performed in the Prism software (version 5.0; GraphPad) and Excel software (Microsoft)

References

1. Jin SL, Conti M. Induction of the cyclic nucleotide phosphodiesterase PDE4B is essential for LPS-activated TNF-alpha responses. *Proc Natl Acad Sci U S A*. 2002;99(11):7628-7633.
2. Harris AW, Pinkert CA, Crawford M, Langdon WY, Brinster RL, Adams JM. The E mu-myc transgenic mouse. A model for high-incidence spontaneous lymphoma and leukemia of early B cells. *J Exp Med*. 1988;167(2):353-371.
3. Kim SW, Rai D, Aguiar RC. Gene set enrichment analysis unveils the mechanism for the phosphodiesterase 4B control of glucocorticoid response in B-cell lymphoma. *Clin Cancer Res*. 2011;17(21):6723-6732.
4. Kim SW, Rai D, McKeller MR, Aguiar RC. Rational combined targeting of phosphodiesterase 4B and SYK in DLBCL. *Blood*. 2009;113(24):6153-6160.
5. Smith PG, Wang F, Wilkinson KN, et al. The phosphodiesterase PDE4B limits cAMP-associated PI3K/AKT-dependent apoptosis in diffuse large B-cell lymphoma. *Blood*. 2005;105(1):308-316.
6. Bouamar H, Jiang D, Wang L, Lin AP, Ortega M, Aguiar RC. MicroRNA 155 Control of p53 Activity Is Context Dependent and Mediated by Aicda and Socs1. *Mol Cell Biol*. 2015;35(8):1329-1340.
7. Ortega M, Bhatnagar H, Lin AP, et al. A microRNA-mediated regulatory loop modulates NOTCH and MYC oncogenic signals in B- and T-cell malignancies. *Leukemia*. 2015;29(4):968-976.

8. Jung I, Aguiar RC. MicroRNA-155 expression and outcome in diffuse large B-cell lymphoma. *Br J Haematol*. 2009;144(1):138-140.
9. Luo Y, Zhou H, Liu L, et al. The fungicide ciclopirox inhibits lymphatic endothelial cell tube formation by suppressing VEGFR-3-mediated ERK signaling pathway. *Oncogene*. 2011;30(18):2098-2107.
10. Weidner N. Current pathologic methods for measuring intratumoral microvessel density within breast carcinoma and other solid tumors. *Breast Cancer Res Treat*. 1995;36(2):169-180.
11. Norrby K, Ridell B. Tumour-type-specific capillary endothelial cell stainability in malignant B-cell lymphomas using antibodies against CD31, CD34 and Factor VIII. *APMIS*. 2003;111(4):483-489.
12. Korkolopoulou P, Thymara I, Kavantzas N, et al. Angiogenesis in Hodgkin's lymphoma: a morphometric approach in 286 patients with prognostic implications. *Leukemia*. 2005;19(6):894-900.
13. de Bont ES, Rosati S, Jacobs S, Kamps WA, Vellenga E. Increased bone marrow vascularization in patients with acute myeloid leukaemia: a possible role for vascular endothelial growth factor. *Br J Haematol*. 2001;113(2):296-304.
14. Liapis K, Clear A, Owen A, et al. The microenvironment of AIDS-related diffuse large B-cell lymphoma provides insight into the pathophysiology and indicates possible therapeutic strategies. *Blood*. 2013;122(3):424-433.
15. Lenz G, Wright G, Dave SS, et al. Stromal gene signatures in large-B-cell lymphomas. *N Engl J Med*. 2008;359(22):2313-2323.
16. Cardesa-Salzmann TM, Colomo L, Gutierrez G, et al. High microvessel density determines a poor outcome in patients with diffuse large B-cell lymphoma treated with rituximab plus chemotherapy. *Haematologica*. 2011;96(7):996-1001.

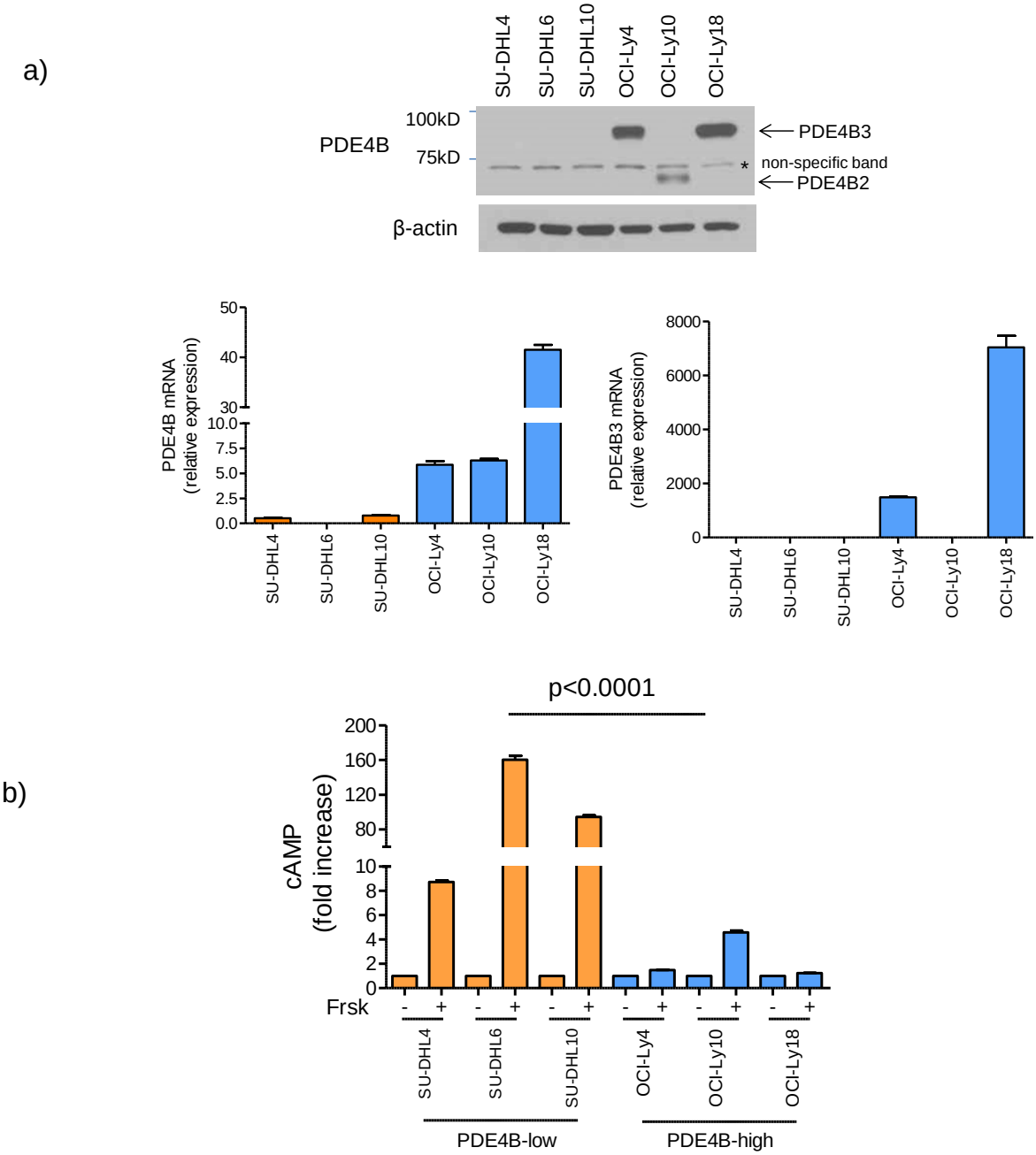

Supplementary Figure 1. Correlation between PDE4B expression and activity. **a)** PDE4B expression was determined by western blot analysis (top) and real-time RT-PCR (Q-RT-PCR, bottom). Western blotting identified two of the principal PDE4B isoforms, PDE4B2 and PDE4B3 in the PDE4B-high DLBCL cell lines, whereas no PDE4B protein was detected in the PDE4B-low cell lines. This protein expression pattern was confirmed by Q-RT-PCR using a set of primers common to all isoforms of the *PDE4B* gene(left), whereas the identity of the larger PDE4B protein in OCI-Ly4 and OCI-Ly18 was confirmed to be *PDE4B3* with the use of primers specific for this isoform (right). The *PDE4B1*-specific Q-RT-PCR did not yield any product in these cell lines. The *PDE4B* expression was normalized to that of a housekeeping gene TBP and relative quantification achieved by calculating $\Delta\Delta$Ct, and expression defined as $2^{-\Delta\Delta Ct}$. **b)** Brief exposure to the adenylyl-cyclase activator Forskolin (40 μM, 30 minutes) was significantly more efficacious in elevating the intracellular levels of cAMP in PDE4B-low than in PDE4B-high DLBCL cell lines ($p<0.0001$, ANOVA; $p<0.01$ Bonferroni's multiple comparison post-test for PDE4B-low cell lines, non-significant for PDE4B-high cells). Data shown are mean ±SD of the fold-increase in cAMP level following Forskolin exposure obtained in an assay performed in triplicate.

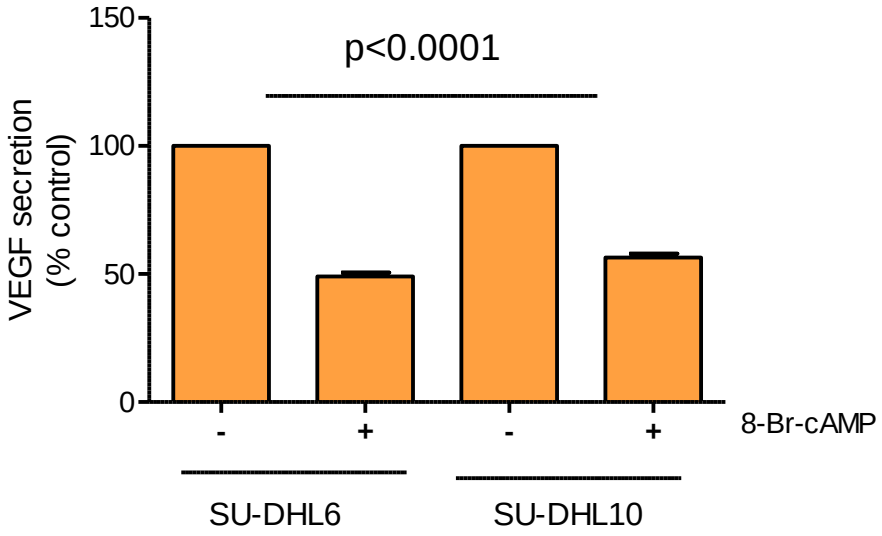

Supplementary Figure 2. Synthetic cAMP recapitulates Forskolin effects towards VEGF in DLBCL cell lines. Exposure of DLBCL to the cell-permeable 8-Br-cAMP resulted in significant suppression of VEGF levels in the supernatant of DLBCL cell lines ($p<0.0001$, ANOVA). Data shown are the mean ± SD of an assay performed in triplicate. Two to three biological replicates were completed.

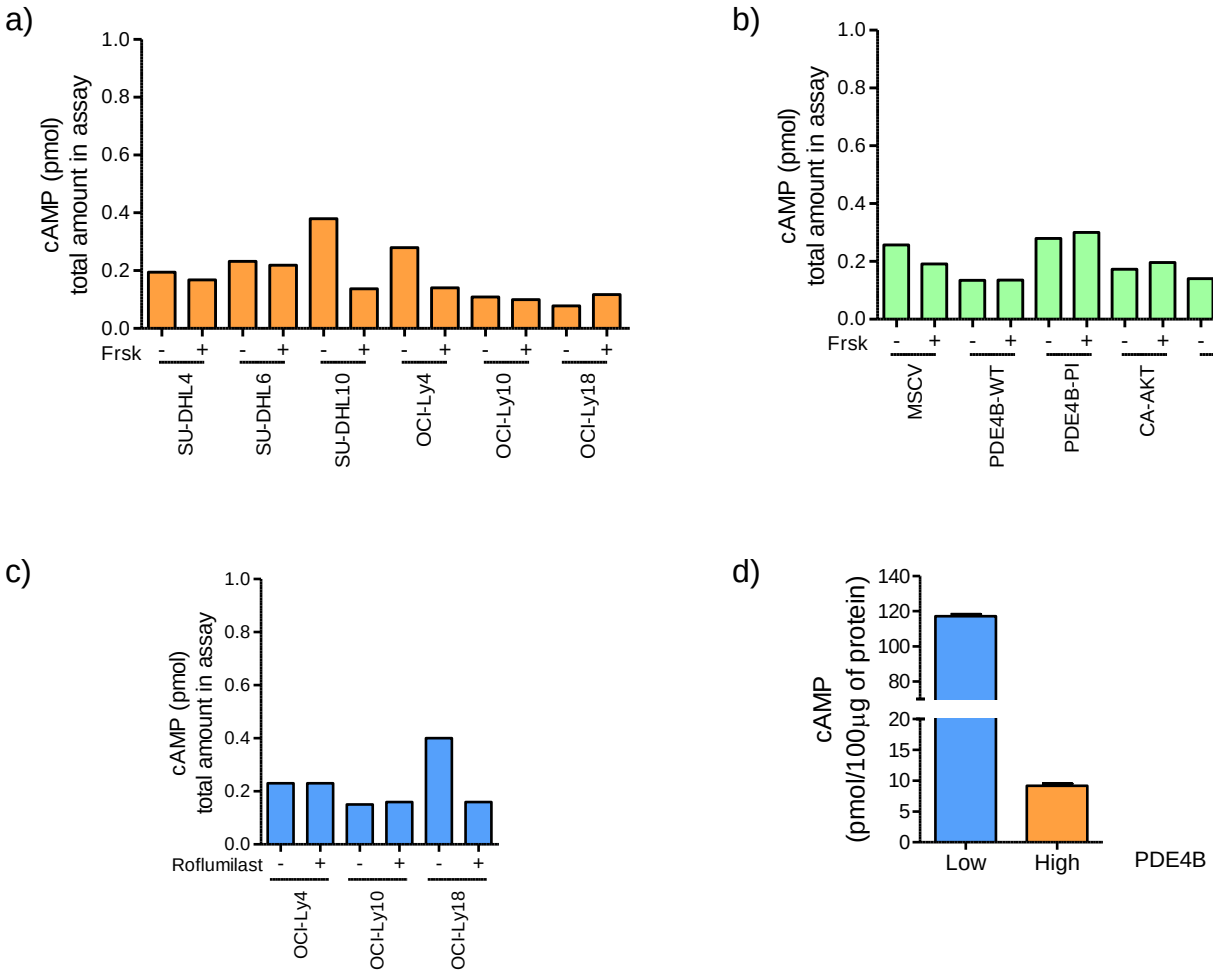

Supplementary Figure 3. Cyclic-AMP quantification in the conditioned media used for HUVEC tube formation assays. We quantified cAMP in the conditioned media obtained from parental DLBCL cell lines (a), from genetic models of gain or loss of function of PDE4B (b), and from DLBCL cell lines treated with Roflumilast (c). As expected, we detected only negligible sub-pmol amounts of cAMP in these samples and the minimal variation across cell lines, when present, did not correlate with the results of the tube formation assays. The values shown represent to the total amount of cAMP present in the 200µm of conditioned media used in the HUVEC assay. Note that the drug labeling (Frsk = Forskolin or Roflumilast) in each display serves simply the purpose of indicating the previous pharmacological modulation, since in all instances, as detailed in the manuscript text, the media-containing media were removed, the cells extensively washed, and the cell culture replenished with drug-free media 24h before collection for use in the HUVEC assays. For comparison purposes, we show in (d), that the amount of intracellular cAMP detected in representative DLBCL cell lines reaches high pmol/mg of protein.

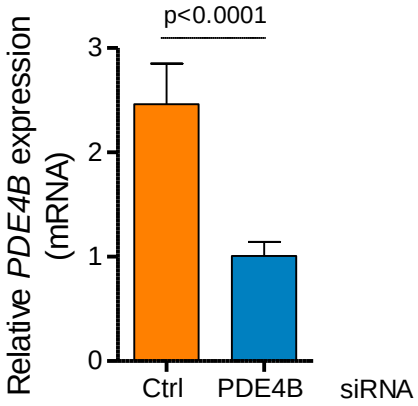

Supplementary Figure 4. SiRNA-mediated suppression of *PDE4B* expression. Quantitative real-time RT-PCR shown an approximate 60% decrease in *PDE4B* expression in the PDE4B-high OCI-Ly18 cell line 48 hours after transfection of control or *PDE4B*-specifc siRNA oligonucleotides (200nM). PDE4B expression was normalized to that of a housekeeping gene TBP, and relative quantification achieved by calculating $\Delta\Delta$Ct, and expression defined as $2^{-\Delta\Delta Ct}$, where control siRNA cells represent the baseline. Data shown are the mean ± SD of a representative assay performed in triplicate - three independent biological replicates were completed and yielded similar results ($p<0.0001$, two-tailed Student's t-test). This assay correlates with the PDE4B knock-down detected by Western blot and showed in the main Figure 2b.

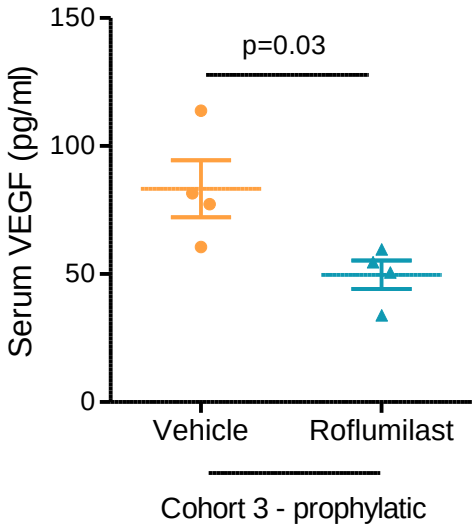

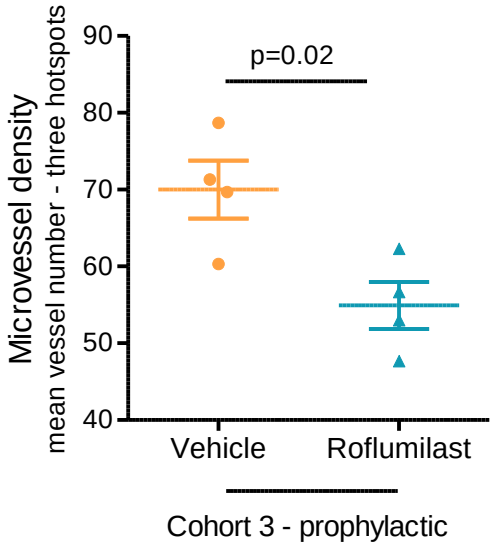

Supplementary Figure 5. Prophylactic administration of Roflumilast suppresses VEGF and angiogenesis in a mouse model of B cell lymphoma. Left - the circulating levels of VEGF were significantly diminished in mice treated with Roflumilast (5mg/kg) when compared to those receiving a vehicle control (p=0.03, two-tailed Student's t-test). Right - the microvessel density was significantly decreased in B cell lymphomas from Roflumialst-treated mice when compared to isogenic tumors that developed in vehicle control-treated mice (p=0.02, two-tailed Student's t-test). In this cohort, treatment started 5 days post B cell lymphoma cells transplant, before the tumors were clinically evident. Data shown are mean ± SEM of data obtained in 8 mice.

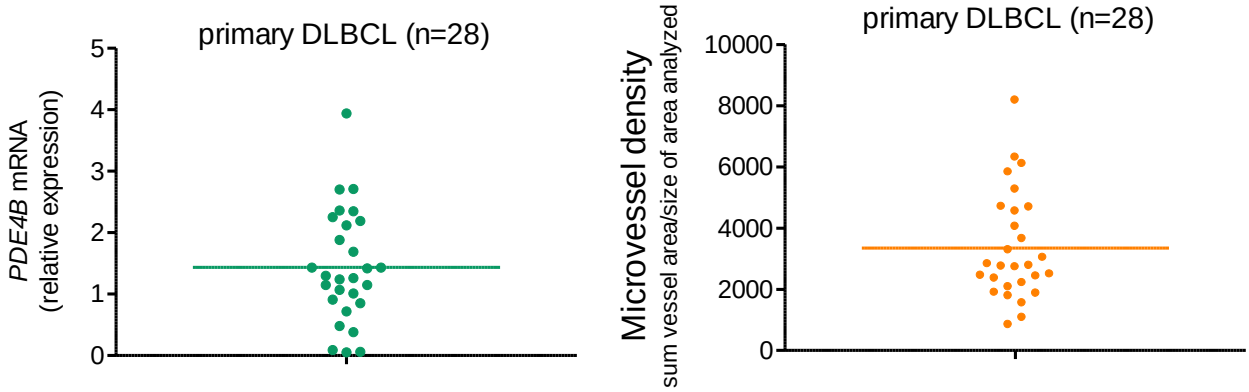

Supplementary Figure 6. *PDE4B* expression and MVD in primary human DLBCL biopsies. Range of expression of *PDE4B* (left) and MVD in DLBCL is shown. Each dot represent an individual tumor and the mean expression or MVD in the entire group s indicated by the horizontal bar. PDE4B expression was determined by Q-RT-PCR performed in triplicate and the MVD for each tumor was defined as the sum of the vessel area divided by the size of the area analyzed.

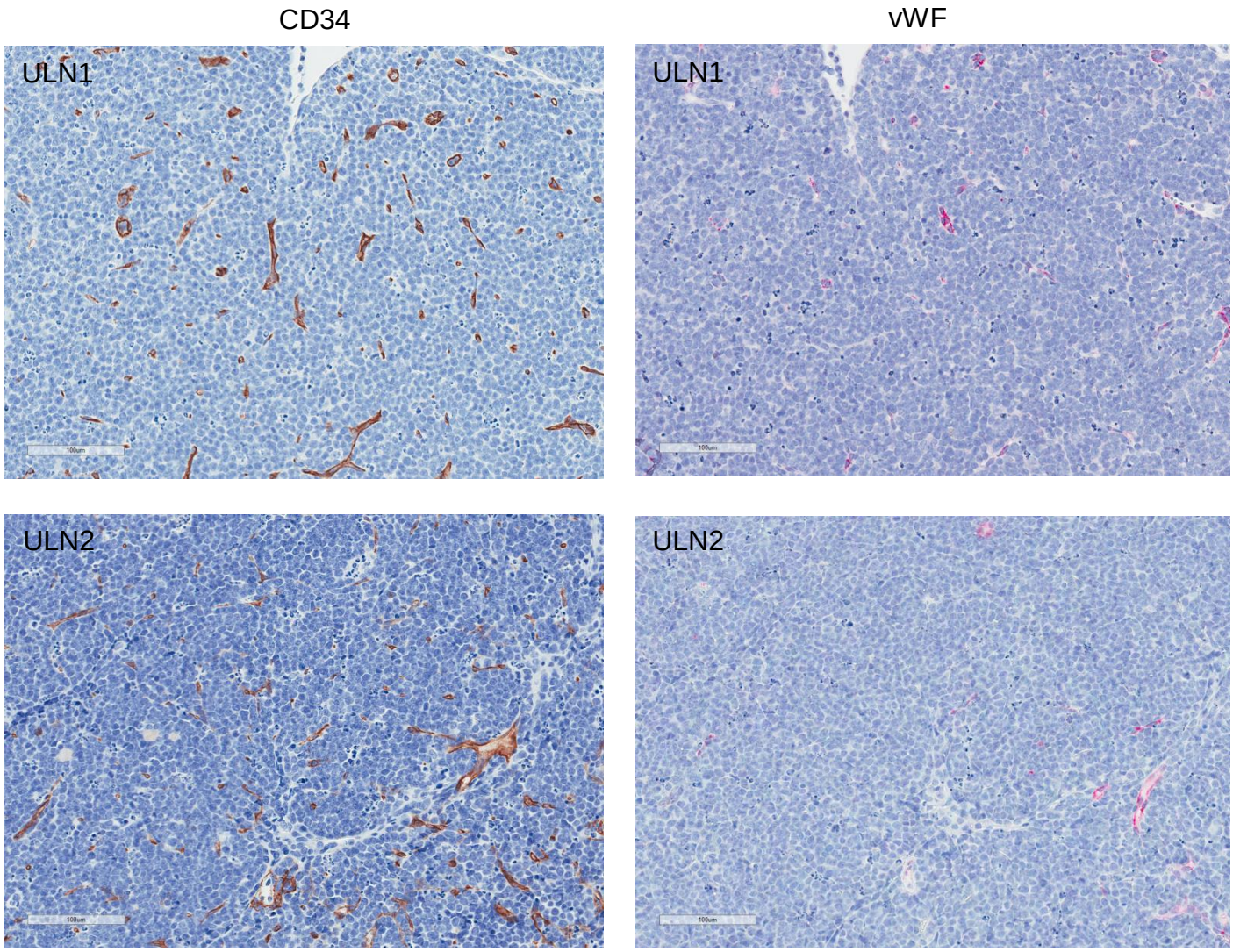

Supplementary Figure 7. Comparison of anti-CD34 and anti-vWF stain in murine B cell lymphomas. The approximately same areas of two representative lymphomas (ULN1 and ULN2) were stained for CD34 (left) and vWF (right panels). CD34 consistently showed a more uniform staining, whereas vWF was overall fainter with more variable intensity. The size bar indicates 100 µm

Table 1. Clinical and immunophenotypic features of lymphomas in *Pde4b*+/+ and *Pde4b*-/- mice

Mouse ID	Genotype	Sex	Survival (days)*	Immunophenotype (%B220/IgM +cells)
C31	*Pde4b+/+;Eμ-Myc-Tg*	M	89	77/36
C83L	*Pde4b+/+;Eμ-Myc-Tg*	F	84	na/65
C97	*Pde4b+/+;Eμ-Myc-Tg*	M	90	na/57
C7R	*Pde4b+/+;Eμ-Myc-Tg*	F	105	94/na
C11	*Pde4b+/+;Eμ-Myc-Tg*	F	75	60/00
C57	*Pde4b+/+;Eμ-Myc-Tg*	F	48	94/32
C18	*Pde4b+/+;Eμ-Myc-Tg*	M	233	na/na
C54	*Pde4b+/+;Eμ-Myc-Tg*	M	130	81/33
C70	*Pde4b+/+;Eμ-Myc-Tg*	F	87	97/54
C54L	*Pde4b+/+;Eμ-Myc-Tg*	M	68	93/42
C58	*Pde4b+/+;Eμ-Myc-Tg*	F	75	na/na
BC116	*Pde4b-/-;Eμ-Myc-Tg*	F	73	92/77
BC114	*Pde4b-/-;Eμ-Myc-Tg*	M	85	91/67
BC86	*Pde4b-/-;Eμ-Myc-Tg*	F	51	93/52
BC85	*Pde4b-/-;Eμ-Myc-Tg*	F	71	na/93
BC51	*Pde4b-/-;Eμ-Myc-Tg*	M	168	97/77
BC89	*Pde4b-/-;Eμ-Myc-Tg*	F	101	90/94
BC111	*Pde4b-/-;Eμ-Myc-Tg*	M	86	61/56
BC12	*Pde4b-/-;Eμ-Myc-Tg*	F	62	64/60

* The Eμ-Myc-Tg; Pde4b+/+ and Eμ-Myc-Tg; Pde4b-/- mice display similar survival profiles

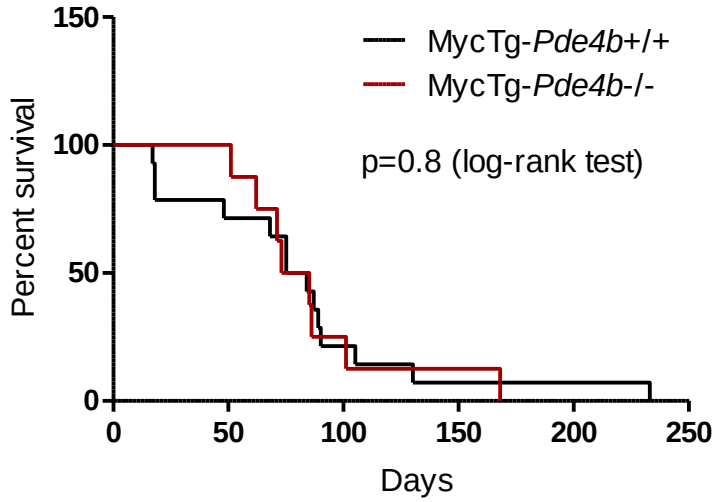

Supplementary Table 2: Oligonucleotide sequences

Gene name	**Sequence (5′-3′)**
Human VEGF	Forward: GGGCAGAATCATCACGAAGT
	Reverse: TGGTGATGTTGGACTCCTCA
Human TBP	Forward: TATAATCCCAAGCGGTTTGCTGCG
	Reverse: AATTGTTGGTGGGTGAGCACAAGG
Human PDE4B (common)	Forward: AGCCCAATGTGTGATAAACA
	Reverse: GACTTGTCTTCTGTTGCAAT
Human PDE4B1	Forward: GTGTCAGCAAACTGCATTG
	Reverse: CTGTAGGATTTACTCAAGC
Human PDE4B3	Forward: CACCAAGGAACTCACCATGC
	Reverse: GAAGGGCCATTTTCCACATC